International Refereed Journal of Engineering and Science (IRJES)
ISSN (Online) 2319-183X, (Print) 2319-1821
Volume 14, Issue 5 (Sep. – Oct. 2025), PP. 25-34

fNIRS data from the prospective of network theory

Xhilda Dhamo[1], Eglantina Kalluçi[1], Eva Noka[1]
[1]*Department of Applied Mathematics, Faculty of Natural Sciences, University of Tirana, Tirana, Albania*

Abstract: *We analyze visibility networks constructed from signals captured from functional Near-Infrared Spectroscopy Data Acquisition and Pre-processing technology (fNIRS) making use of properties of network theory with the aim to characterize the network properties of fNIRS visibility networks. The fNIRS technology is used to capture the brain activity of dyads of two persons by measuring the oxyhemoglobin (HbO) level during a task called "MapTask". Our approach consists in three consecutive steps: (i) firstly, we employe a sliding window technique to segment fNIRS signals; (ii) secondly, we convert the HbO signals in each sliding window to visibility networks; (iii) thirdly, we employ network properties such as diameter, clustering coefficient, assortativity, transitivity and density across different cerebral time windows. Furthermore, we investigate the degree distribution of the nodes in the networks and it is observed that they follow a power- law distribution as the length of the signal increased suggesting scale- free characteristics.*
Keywords*: fNIRS, oxyhemoglobine signals, visibility networks, brain acitivity*

Date of Submission: 08-09-2025 Date of acceptance: 19-09-2025

I. INTRODUCTION

Network theory is lastly ranked as a powerful tool in the identification and prediction of the different collective phenomena in various complex systems (Boccaletti et al. 2006; Arenas et al. 2008; Barrat et al. 2008; Halvin et al. 2012; Chen et al. 2015; Newman, 2018). In previous research papers (Dhamo et al. 2024a; Dhamo et al. 2024b) we have addressed the dynamic phenomena of synchronization in the fNIRS visibility networks, whereas here we try to explore the properties of the visibility networks. The network properties like diameter, clustering coefficient, assortativity, transitivity and density have been widely used to investigate and analyze complex phenomena after modelling them as networks (Estrada and Knight, 2018; Newman, 2018).

Visibility network, firstly proposed by (Lacasa et al. 2008) is an important technique to convert a time series into a network. In the literature, there are two different approaches related to the construction of the visibility network: (i) natural visibility network (Lacasa et al. 2008); and (ii) horizontal visibility network (Luque et al. 2009), which is a simplified version of the first mentioned (i). Both of them, have the same main characteristics: (i) the visibility network is connected; (ii) undirected; (iii) invariant from the affine transformation of the time series data; and (iv) it can be used in all kind of time series data (Lacasa et al. 2008; Luque et al. 2009; Lacasa et al. 2012; Lacasa et al. 2015). Their application in the neuroscience is focused to EEG data (Mira- Iglesias et al. 2016, Bhaduri& Ghosh 2016), fMRI data (Sannino et al. 2017) and fNIRS data (Dhamo et al. 2024a; Dhamo et al. 2024b).

In this paper, we use visibility graphs to map fNIRS time series data into networks and explore the time series from the network theory prospective. fNIRS is a technology used to measure brain activity through the levels of the HbO captured in the head of participants following a certain experiment (Li et al. 2021). The HbO signals are registered by the optods positioned in left and right hemispheres of the prefrontal cortexes (PFC) of the participants in the experiment. Recent publications in this area have addressed their importance in estimating the brain synchronization of individuals when collaborating to complete a particular task (Li et al. 2021; Wang et al. 2022). In this paper, we follow a different approach. Firstly, we segment the fNIRS time series during a particular time of the experiment duration and convert visibility networks. In addition, we compute the diameter, density, clustering coefficient, transitivity, modularity, assortativityand compare the results for different sliding windows. Furthermore, we consider increasing sliding windows for the time series, from 1 minute up to 20 minutes of experiment duration and investigate the node degree distribution. Experimental results suggest that the degree distribution follows the power law distribution with the increasing of experiment time duration considered.

The rest of the paper is organized as follows. In the second section we present the network theory background focusing in the concepts of diameter, density, clustering coefficient, transitivity, modularity and assortativitythat we will use in the following experimental section. Furthermore, we introduce the visibility graph approach. The third section describes the generation of the data and provides the experimental results

obtained from our analysis. Conclusions summaries all the word conducted and results obtained from our investigation.

II. MATHEMATICAL BACKGROUND

2.1Fundamentals in networks

The mathematical notations related to graph theory are a summary of notations presented in numerous number of scientific papers in this field (Estrada and Knight, 2018; Newman, 2018). Throughout this paper, we will use the notations graph and network as a synonym of each- other. Here, we define a network as a pair $G = (V, E)$, where V is called the vertex set and E refers to the edge set. This study is limited to undirected networks where E is a symmetric set and unweighted networks. A network is uniquely defined by its adjacency matrix A defined as A: $\mathrm{a_{ij}} = \begin{cases} 1 & (\mathrm{i,j}) \in \mathrm{E} \\ 0 & (\mathrm{i,j}) \notin \mathrm{E} \end{cases}$. $A$is a binary matrix in case of unweighted networks. The degree of a node in a network is the number of edges incident to that particular node. In addition, the degree distribution refers to the statistical representation, which gives the relative frequency of each degree value within the network. In other words, the degree distribution $P(k)$ is the probability that a randomly selected node is incident to exactly k edges.In the literature,there exist various network models based on the degree distribution: (i) regular graphs which degree distribution is defined as $P(d) = \delta(d - k)$ (ii) random networks, whose nodes degree distribution follows the Poisson distribution $P(k) = \frac{e^{-\lambda}\lambda^k}{k!}$ and they are referred as Erdós–Rényi networks (iii) scale- free networks, whose node degree distribution follows the power- law distribution $P(k) \propto k^{-\gamma}$, where γ is the power- law exponents. In case of, scale- free networks $2 \leq \gamma \leq 3$.

Let's consider a network $G = (V, E)$. A path in the network is a sequence of edges, which joins a sequence of distinct vertices in the network. In addition, the shortest path between two vertices is defined as the path between that particular vertices which has the minimum number of edges and we refer as $d(i, j)$. Furthermore, the diameter of G is the length of the longest shortest path between any pair of nodes:

$$diam(G) = \max_{i,j \in V} d(i, j) \qquad (1)$$

Density measures how many edges exist in the network compared to the maximum number of edges:

$$density(G) = \frac{2|E|}{|V|(|V| - 1)} \qquad (2)$$

Density indicates how 'connected' a network is, with values range from 0, indicating a disconnected network to 1, which indicates a complete network.

Furthermore, local clustering coefficient of a node i in G quantifies how close the neighbors of a vertex are to being a clique (complete graph):

$$C_i = \frac{2e_i}{k_i(k_i - 1)} \qquad (3)$$

wheree_i refers to edge i and k_i refers to the degree of node i.

Whereas, the average clustering coefficient evaluates the degree to which nodes in a network tend to cluster together:

$$C = \frac{1}{|V|}\sum_{i \in V} C_i \qquad (4)$$

Lastly, the transitivity, also called the global clustering coefficient measures the overall level of clustering in the network:

$$T = \frac{3 \times number\ of\ triangels}{number\ of\ connected\ triplets\ of\ nodes} \qquad (5)$$

Modularity is defined as the number of edges falling within groups minus the expected number in an equivalent network with edges placed at random (Newman et al. 2006):

$$Q = \frac{1}{2m}\sum_{i,j}\left[A_{ij} - \frac{k_i k_j}{2m}\right]\delta(c_i, c_j) \qquad (6)$$

where$m$ is the total number of edges, c_i is the community assignment of node i and $\delta(c_i, c_j) = 1$, if node i dhe j belongs to the same community and 0 otherwise. Higher values of Q indicates stronger community structure.

Degree assortativity measures the correlation between the degrees of connected nodes:

$$r = \frac{\sum_{i,j}\left(A_{ij} - \frac{k_i k_j}{2m}\right)k_i k_j}{\sum_{i,j}\left(k_i\delta_{ij} - \frac{k_i k_j}{2m}\right)k_i k_j} \qquad (7)$$

where $r > 0$ indicates that network is assortative, which means that high- degree nodes tend to connect to high- degree nodes and same for low- degree nodes; $r < 0$ indicates that network is dissassortative, which means that high- degree nodes tend to connect to low- degree nodes; and $r = 0$ indicates that there is no degree correlation in the network.

A network G exhibits the small- world property if it has small value of the average shortest path length and high value of the clustering coefficient (Estrada and Knight, 2018; Newman, 2018).

2.2 Visibility network

The visibility network approach, which converts a time series into a network,was firstly proposed by (Zhang and Small, 2006) and its disadvantages is that its application is limited only to pseudoperiodic time series. Two years later, (Lacasa et al. 2008) proposed a new approach for visibility network, which can be applied to every kind of time series data. Let's consider a time series with Ndata measured at times$t_i, i = 1, 2, \ldots, N$ with values $x_i, i = 1, 2, \ldots, N$ and consecutive time points(t_i, x_i), (t_k, x_k) and (t_j, x_j). Time points (t_i, x_i) and $(t_j, x_j)$are visible and consequently will become two connected nodes in the visibility graph if for any point(t_k, x_k)between them, they fulfill the following inequation (8):

$$x_k < x_j + (x_i - x_j)\frac{t_j - t_k}{t_j - t_i} \qquad (8)$$

The construction of the natural visibility graph is illustrated schematically in figure 1 given a time series with *N*=20.

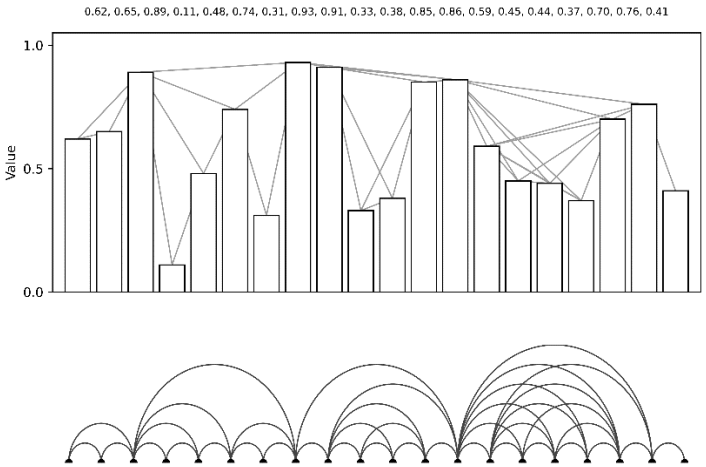

Fig. 1. Natural visibility network

One year later (Luque et al. 2009) proposed a simplified version of the natural visibility network, called horizontal visibility network, which is defined as follows. Let's consider a time series with N data measured at

times $t_i, i = 1, 2, \dots, N$ with values $x_i, i = 1, 2, \dots, N$ and consecutive time points (t_i, x_i), (t_k, x_k) and (t_j, x_j). Time points (t_i, x_i) and (t_j, x_j) are visible and consequently will become two connected nodes in the visibility graph if for any point (t_k, x_k) between them, they fulfill the following inequation (9):

$$x_i, x_j > x_k, \qquad \forall n: i < n < j \tag{9}$$

The horizontal visibility graph presents a subgraph of the natural visibility graph. Figure 2 illustrates the construction of the horizontal visibility graph from the same time series as presented in figure 1.

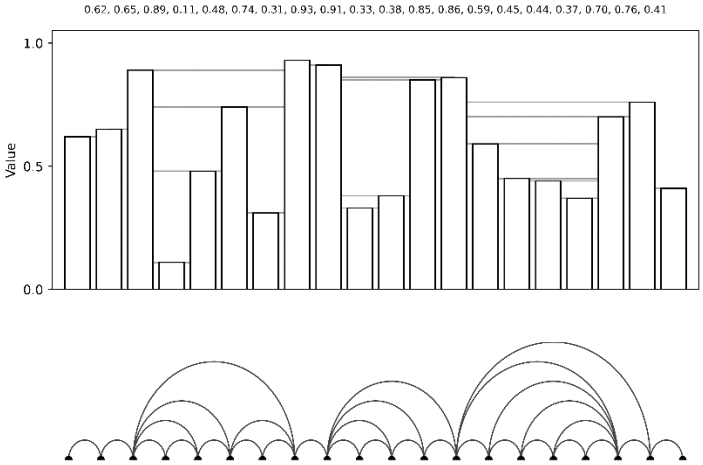

Fig. 2. Horizontal visibility network

III. EXPERIMENTAL RESULTS

3.1 Experiment setup

A collaborative task known as "MapTask" was assigned to two participants, thereby forming a dyad. The guiding participant (pA) was presented with 35 icons and a predefined path displayed on their screen, while the following participant (pB) was shown the same set of icons but without the path. The objective of the experiment was that, by the conclusion of the task, pB would reproduce the same path visible on pA's screen by using the keyboard arrows, based on the verbal instructions provided by pA.

Brain activity was recorded using Functional Near-Infrared Spectroscopy (fNIRS) with data acquisition and preprocessing procedures. Each participant was equipped with two optodes placed on the prefrontal cortex (PFC): one in the left hemisphere (hL) and the other in the right hemisphere (hR). These optodes measured both oxyhemoglobin (HbO) and deoxyhemoglobin (HbR) concentration changes. Since HbOis considered more responsive to variations in cerebral blood flow compared to HbR, our analysis focused on the HbO signal (Wang et al., 2022). A total of 18 participants were recruited and organized into 9 dyads. For analysis, we considered the first five minutes of data collection at the onset of the experiment. The cooperative task performed at the beginning of the experiment and after completing it, is illustrated in Figure 3 and 4 respectively.

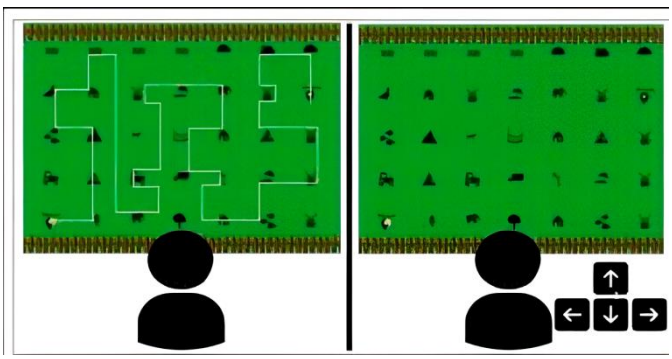

Fig. 3. "MapTask" view at the beginning of the experiment

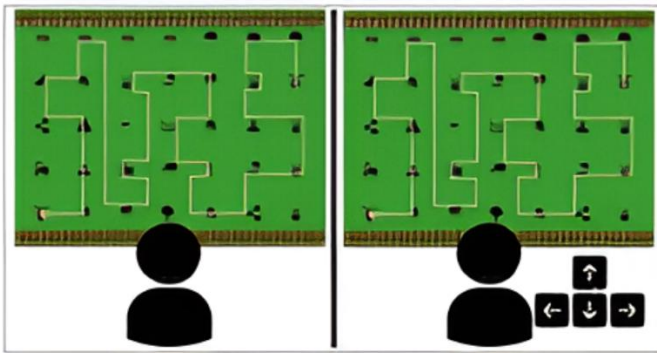

Fig. 4. "MapTask" view at the end of the experiment.

3.2 Brain network properties

The HbO time series are mapped into visibility networks as described in section 2. There are two networks for each participant, corresponding to the signals obtained by measuring theHbO in left (lPFC) and right prefrontal cortex hemispheres (rPFC). For simplicity, from now on we will refer as pAhL (pAhR) the lPFC (rPFC) HbO signals of pA and as pBhL (pBhR) the lPFC (rPFC) HbO signals of pB. In addition, we divide the time series into non- overlapping segments of 5 seconds each and construct the natural visibility network for each sliding window. Furthermore, the network properties are computed in each network and visualized in the following figures.

Figure 5 illustrates the diameter value computed for network in each sliding window.

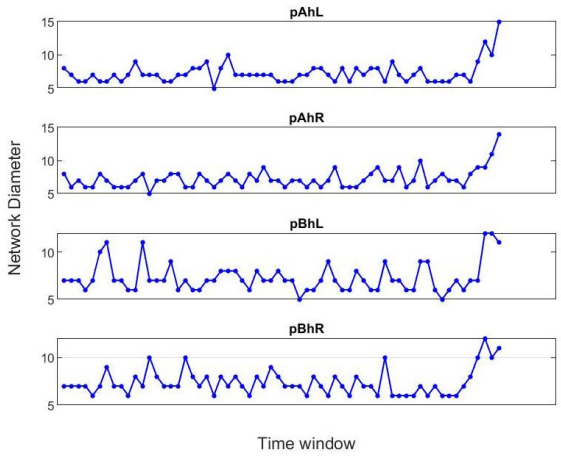

Fig. 5. Diameter for each window visibility network

The plots show the evolution of the network diameter across time windows for each hemisphere of the guide (pA) and follower (pB) participants.In pA's networks (pAhL, pAhR), the diameter remains relatively stable for most windows, followed by a noticeable increase toward the end of the task, suggesting higher dispersion or reduced efficiency in connectivity. For pB's networks (pBhL, pBhR), stronger fluctuations are observed throughout, indicating less stable structural patterns during task execution. Overall, the results suggest that while both participants show an increase in diameter near the end, the follower's networks display greater variability compared to the guide's more consistent dynamics.

Figure 6 illustrates the density value computed for network in each sliding window. The plots display how network density evolves across time windows for the guide (pA) and follower (pB) participants in both hemispheres. In the guide's networks (pAhL, pAhR), density values remain relatively stable around 0.07, with small fluctuations and a slight decline toward the end, suggesting a modest reduction in connectivity.The follower's left hemisphere (pBhL) exhibits more variability, with several sharp increases and decreases, indicating unstable structural organization during task execution.The follower's right hemisphere (pBhR) shows frequent low-density fluctuations, reflecting weaker and less consistent connectivity patterns compared to the guide.

Overall, the results highlight that while the guide's networks maintain more stable density, the follower's networks demonstrate stronger variability, particularly in the left hemisphere.

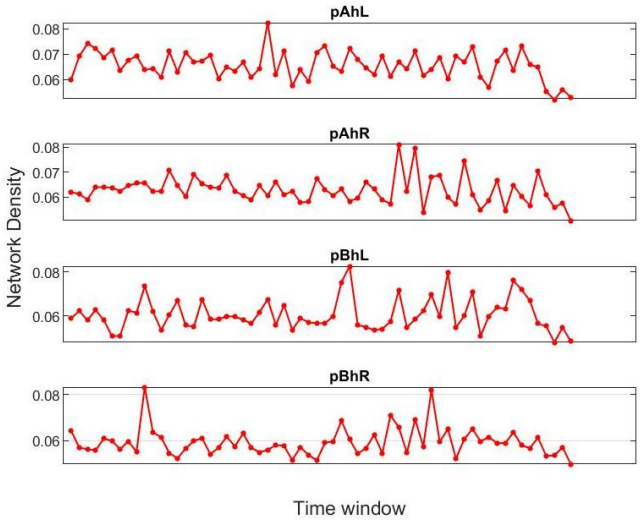

Fig. 6. Density for each window visibility network

Figure 7 illustrates the global clustering coefficient value computed for network in each sliding window.

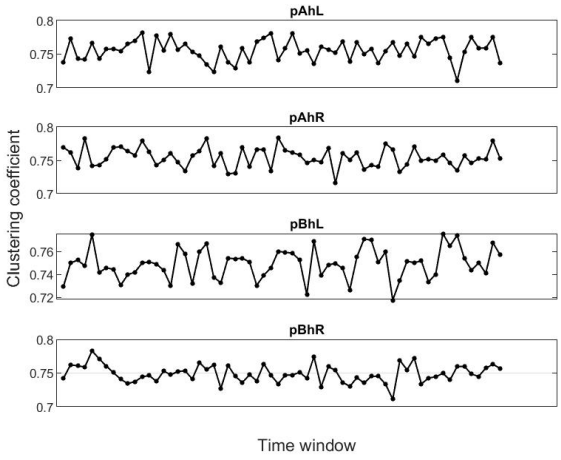

Fig. 7. Clustering coefficient for each window visibility network

The plots illustrate how the clustering coefficient changes over time windows for the guide (pA) and follower (pB) participants in both hemispheres. For the guide (pAhL and pAhR), clustering values remain fairly stable around 0.75, with moderate fluctuations, indicating consistent local interconnectedness among nodes.The follower's left hemisphere (pBhL) shows slightly lower and more variable clustering coefficients compared to the guide, reflecting less stable local network organization.The follower's right hemisphere (pBhR) exhibits smoother trends, with clustering coefficients staying close to 0.75 and fewer sharp deviations than in pBhL.Overall, the guide demonstrates higher stability in clustering across both hemispheres, while the follower's left hemisphere shows greater variability, suggesting possible differences in local coordination during the task.

Figure 8 illustrates the transitivity coefficient value computed for network in each sliding window. The plots present how the transitivity coefficient evolves across time windows for the guide (pA) and follower (pB) participants in both hemispheres.For the guide's networks (pAhL and pAhR), transitivity remains relatively stable around 0.47–0.50, with moderate oscillations and a small upward trend toward the final windows. The follower's left hemisphere (pBhL) shows stronger fluctuations than the guide, with values ranging between 0.41 and 0.50, indicating more unstable local triangle formation. The follower's right hemisphere (pBhR) exhibits the lowest stability overall, with multiple sharp drops near 0.40 but also a late increase toward 0.50, suggesting irregular clustering patterns. Overall, the guide maintains more consistent transitivity across both hemispheres,

whereas the follower shows higher variability, particularly in the right hemisphere, reflecting differences in local structural organization during the cooperative task.

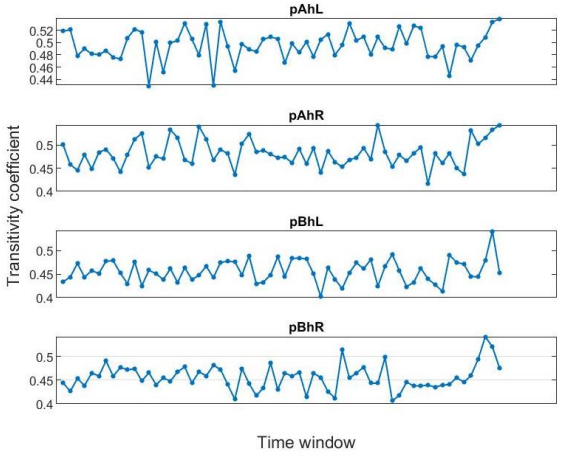

Fig. 8. Transitivity for each window visibility network

Figure 9 illustrates the modularity coefficient value computed for network in each sliding window.

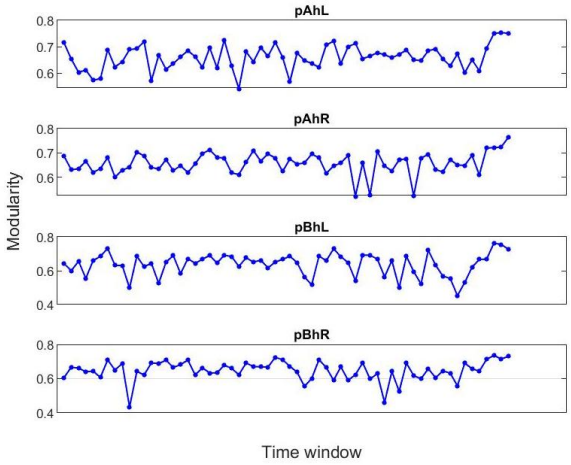

Fig. 9. Transitivity for each window visibility network

The plots illustrate the variation of modularity across time windows for the guide (pA) and follower (pB) participants in both hemispheres. In the guide's networks (pAhL and pAhR), modularity remains fairly stable between 0.65 and 0.72, with a slight upward tendency toward the end, indicating strengthening of community structure. The follower's left hemisphere (pBhL) shows greater fluctuations, with modularity dropping to around 0.55 in some windows but recovering later, suggesting unstable but adaptive community partitioning. The follower's right hemisphere (pBhR) exhibits lower variability, maintaining modularity between 0.60 and 0.70, reflecting more consistent community organization compared to pBhL.Overall, the guide maintains stronger and more stable modular structure, while the follower shows higher variability, particularly in the left hemisphere, which may reflect differences in cognitive load during the cooperative task.

Figure 10 illustrates the assortativity coefficient value computed for network in each sliding window. The plots depict the evolution of the assortativity coefficient across time windows for the guide (pA) and follower (pB) participants in both hemispheres. In the guide's networks (pAhL and pAhR), assortativity remains mostly positive, ranging between 0.1 and 0.2, with occasional peaks near 0.3, indicating a general tendency for nodes to connect with others of similar degree.The follower's left hemisphere (pBhL) displays stronger variability, with assortativity dropping close to zero toward the end, suggesting weakened degree–degree correlations over time.The follower's right hemisphere (pBhR) also shows irregular fluctuations, with multiple instances near zero assortativity, reflecting unstable patterns of connectivity preferences.Overall, the guide demonstrates more consistent assortative mixing, while the follower's networks—particularly in the left hemisphere—show higher instability and reduced assortativity toward the end of the task.

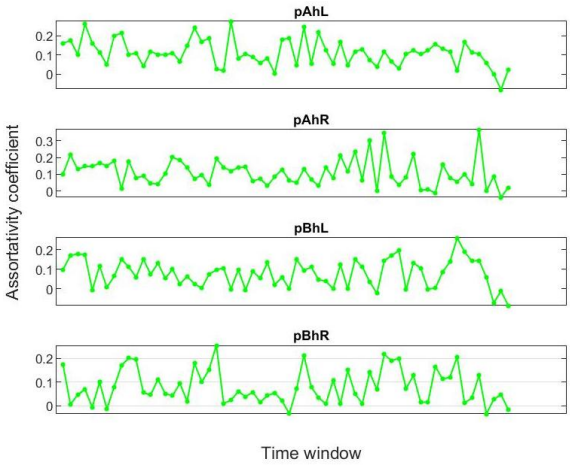

Fig. 10. Transitivity for each window visibility network

Table 1 summaries the average diameter, density, clustering coefficient, transitivity, modularity and assortativity across all time windows for all pAhL, pAhR, pBhL and pBhR participants.

Table 1. Average network properties

Participant	Average Diameter	Average density	Average Clustering Coefficient	Average Transitivity	Average Modularity	Average assortativity
pAhL	7.2742	0.0656	0.7558	0.4958	0.6605	0.1101
pAhR	7.2581	0.0627	0.7545	0.4818	0.6565	0.1088
pBhL	7.3871	0.0605	0.7493	0.4560	0.6377	0.0791
pBhR	7.3065	0.0593	0.7490	0.4560	0.6470	0.0808

Lastly, we consider increasing sliding windows for the time series, from 1 minute up to 20 minutes of experiment duration and investigate the node degree distribution. Figure 11-13 illustrates the degree distribution of the visibility networks corresponding to 1, 2 , 3, 4, 10 and 20 minutes respectively.

Across all time windows (1, 2, 3, 4, 10, and 20 minutes), the log–log plots of node degree distributions consistently show heavy-tailed patterns, indicative of scale-free–like behavior where most nodes have low degree and only a few nodes achieve high degree. In the early stages (1–2 minutes), the distributions drop off more steeply, suggesting a faster decay and fewer high-degree nodes. As time increases (3–4 minutes), the distributions begin to flatten slightly, with a broader spread of node degrees and clearer alignment with a power-law trend. At 10 minutes, the power-law fit becomes more evident, with higher-degree nodes appearing more frequently and the tail extending further. By 20 minutes, the network exhibits the broadest distribution, with the longest tail and the highest number of hubs, confirming that as the time window grows, the network accumulates more links, leading to stronger scale-free characteristics and increased heterogeneity.

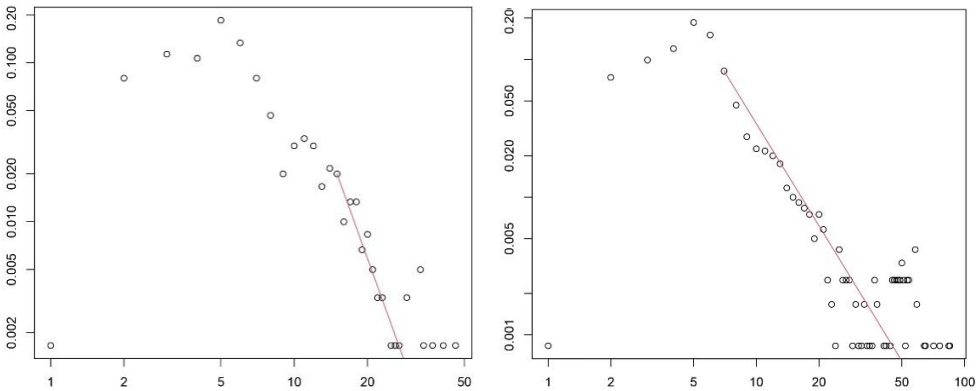

Fig. 11. : Node degree distribution for 1 (left) and 2 minutes (right) visibility networks

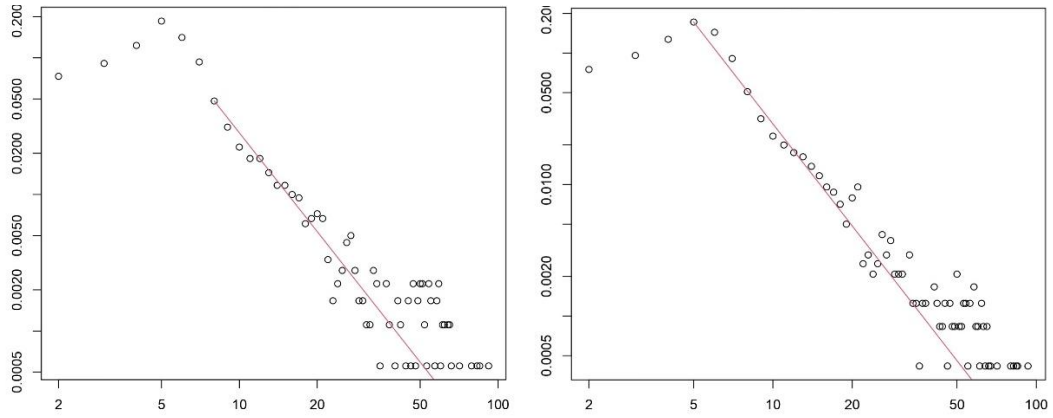

Fig. 12. : Node degree distribution for 3 (left) and 4 minutes (right) visibility networks

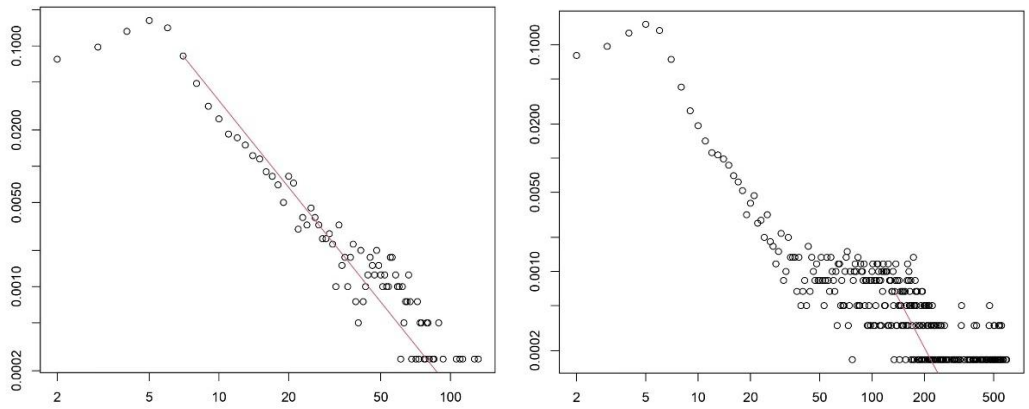

Fig. 13. : Node degree distribution for 10 (left) and 20 minutes (right) visibility networks

Table 2 provides the estimated scaling exponent and p- value for different duration of the experiment.

Table 2. Estimated scaling exponent and p- value for different duration of the experiment

Participant	1 minute	2 minutes	3 minutes	4 minutes	10 minutes	20 minutes
Estimated scaling exponent	4.254379	2.465897	2.402139	2.574566	2.393856	2.905879
p- value	0.9954987	0.03500376	0.03975481	0.02860772	0.04519935	0.9954987

At 1 minute, the estimated scaling exponent is very high ($\gamma \approx 4.25$), suggesting a rapid decay of the degree distribution where hubs are nearly absent. However, the p-value (0.995) is non-significant, indicating that a power-law is not a good fit at this early stage. At 2–4 minutes, the exponents drop into the range $\gamma \approx 2.4$–2.6, which is consistent with typical scale-free networks. Importantly, the p-values (0.035–0.028) are below 0.05, confirming that the power-law model is statistically significant in this interval. This suggests that during these time windows, the network begins to show heavy-tailed degree distributions with clear hub formation. At 10 minutes, the exponent remains close to $\gamma \approx 2.39$, still within the scale-free range. The p-value (0.045) is just below 0.05, indicating marginal but still acceptable statistical support for a power-law fit. At 20 minutes, the exponent increases again ($\gamma \approx 2.91$), reflecting a steeper distribution with fewer extreme hubs. However, the p-value (0.996) indicates a poor fit, suggesting that the degree distribution at longer observation windows deviates from pure power-law behavior, possibly due to saturation effects or alternative heavy-tailed distributions (e.g., truncated power-law, log-normal). The best evidence for scale-free structure occurs between 2 and 10 minutes, with exponents in the critical range ($2< \gamma < 3$) and statistically significant p-values. In contrast, very short (1 min) and very long (20 min) windows do not support a either valid power-law fit, due to insufficient connectivity (early) or structural saturation (late).

IV. CONCLUDING REMARKS

The visibility graph approach transforms time series into complex networks, enabling the extraction of topological features from temporal data (Zhang and Small, 2006; Lacasa et al., 2008; Luque et al., 2009). In this work, HbO signals obtained from fNIRS measurements of participants engaged in the cooperative "MapTask" experiment were mapped into visibility networks. Network measures computed in non-overlapping 5-second windows revealed that the guide (pA) exhibited more stable dynamics across hemispheres, whereas the follower (pB) displayed greater variability, particularly in the left hemisphere, in terms of diameter, density, clustering, transitivity, modularity, and assortativity. Analysis of degree distributions across increasing window lengths (1–20 minutes) demonstrated heavy-tailed patterns indicative of scale-free–like organization. Statistically significant power-law fits were observed between 2 and 10 minutes ($\gamma \approx 2.4$–2.6, $p < 0.05$), confirming the emergence of hubs and scale-free connectivity. In contrast, very short (1 min) and very long (20 min) durations yielded non-significant fits, suggesting either insufficient connectivity or deviations from pure power-law behavior toward alternative heavy-tailed distributions.

REFERENCES

[1]. Arenas, A., Díaz-Guilera, A., Kurths, J., Moreno, Y., Zhou, C.: Synchronization in complex networks. Physics Reports. 469, 93-153 (2008). https://doi.org/https://doi.org/10.1016/j.physrep.2008.09.002

[2]. Barrat, A., Barthélemy, M., Vespignani, A.: Dynamical Processes on Complex Networks. Cambridge University Press (2008).

[3]. Boccaletti, S., Latora, V., Moreno, Y., Chavez, M., Hwang, D.-U.: Complex networks: Structure and dynamics. Physics Reports. 424, 175-308 (2006). https://doi.org/https://doi.org/10.1016/j.physrep.2005.10.009Ahmed J. and Ahamed S. (2014), "Seismic Vulnerability of RC Buildings by Considering Plan Irregularities Using Pushover Analysis", *Globaljournal for research analysis,3*, 2014, 42-47.

[4]. Chen, G., Wang, X., Li, X.: Fundamentals of Complex Networks: Models, Structures and Dynamics. Willey (2015)

[5]. Dhamo X, Kalluçi E, Dray G, et al (2024a) Global Synchronization Measure Applied to Brain Signals Data. In: Studies in Computational Intelligence. Springer, France

[6]. Dhamo X, Kalluçi E, Noka E, et al (2024b) Synchronization processes in fNIRS visibility networks. Applied Network Science 9:.https://doi.org/https://doi.org/10.1007/s41109-024-00663-x

[7]. Estrada, E., Knight, P.A.: A First Course in Network Theory. Oxford University Press (2025)

[8]. Halvin, S., Kenett, D.Y., Ben-Jacob, E., Bunde, A., Cohen, R., Hermann, H., Kantelhardt, J.W., Kertész, J., Kirkpatrick, S., Kurths, J., Portugali, J., Solomon, S.: Challenges in network science: Applications to infrastructures, climate, social systems and economics. The European Physical Journal Special Topics. 273-293 (2012). https://doi.org/https://doi.org/10.1140/epjst/e2012-01695-x

[9]. Lacasa, L., Luque, B., Ballesteros, F., Luque, J., Nuño, J.C.: From time series to complex networks: The visibility graph. Applied Mathematics. 105, 4972-4975 (2008). https://doi.org/https://doi.org/10.1073/pnas.0709247105

[10]. Lacasa, L., Luque, B., Luque, J., Nuño, J.C.: The visibility graph: A new method for estimating the Hurst exponent of fractional Brownian motion. Europhysics Letters. 86, (2009). https://doi.org/10.1209/0295-5075/86/30001

[11]. Lacasa, L., Nicosia, V., Latora, V.: Network structure of multivariate time series. Scientific Reports. 5, (2015). https://doi.org/https://doi. org/10.1038/srep15508

[12]. Lacasa, L., Nuñez, A., Roldán, É.,Parrondo, J.M.R., Luque, B.: Time series irreversibility: a visibility graph approach. The European Physical Journal B. 85, (2012). https://doi.org/https://doi.org/10.1140/epjb/e2012-20809-8

[13]. Li, R., Mayseless, N., Balters, S., Reiss, A.L.: Dynamic inter-brain synchrony in real-life inter-personal cooperation: A functional near-infrared spectroscopy hyperscanning study. NeuroImage. 238, (2021). https://doi.org/https://doi.org/10.1016/j.neuroimage.2021.118263

[14]. Luque B, Lacasa L, Ballesteros F, Luque J (2009) Horizontal visibility graphs: Exact results for random time series. Physical Review E 80:.https://doi.org/https://doi.org/10.1103/PhysRevE.80.046103

[15]. Mira- Iglesias, A., Conejero, J.A., Navarro-Pardo, E.: Natural visibility graphs for diagnosing attention deficit hyperactivity disorder (ADHD). Electronic Notes in Discrete Mathematics. 54, 337-342 (2016). https://doi.org/https://doi.org/10.1016/j.endm.2016.09.058

[16]. Newman, M.: Networks. Oxford University Press (2018)

[17]. M.E.J. Newman, Modularity and community structure in networks, Proc. Natl. Acad. Sci. U.S.A. 103 (23) 8577-8582, https://doi.org/10.1073/pnas.0601602103 (2006).

[18]. Sannino, S., Stramaglia, S., Lacasa, L., Marinazzo, D.: Visibility graphs for fMRI data: Multiplex temporal graphs and their modulations across resting-state networks. Network Neuroscience. 1, 208-221 (2017). https://doi.org/https://doi.org/10.1162/NETN_a_00012

[19]. Wang, X., Zhang, Y., He, Y., Lu, K., Hao, N.: Dynamic Inter-Brain Networks Correspond with Specific Communication Behaviors: Using Functional Near-Infrared Spectroscopy HyperscanningDuring Creative and Non-creative Communication. Frontiers in Human Neuroscience. 16, (2022). https://doi.org/https://doi.org/10.3389/fnhum.2022.907332